ACS Energy LETTERS

http://pubs.acs.org/journal/aelccp

Kinetic Control over Disproportionation Stabilizes Wurster's Blue Catholyte for Nonaqueous Redox Flow Batteries

Xiaoting Fang,[▽] Zhiguang Li,[▽] Lifan Zeng, Heonjae Jeong, Diqing Yue, Lily A. Robertson, Yuyue Zhao, Lei Cheng, Ilya A. Shkrob,* Xiaoliang Wei,* and Lu Zhang*

Cite This: *ACS Energy Lett.* 2024, 9, 5737−5743

Read Online

ACCESS | Metrics & More | Article Recommendations | Supporting Information

ABSTRACT: **Redoxmers are organic molecules that serve as charge carriers in redox flow batteries. While these materials are affordable and easy to source, insufficient stability of their charged states (radical ions) remains a challenge. A common reaction of these species is their disproportionation. This reversible reaction yields unstable multiply charged states, shifting the overall charge transfer equilibrium toward the decomposition products. Here we show how kinetic controls can be engineered into a redoxmer molecule to suppress these unwanted charge transfer reactions. This approach is used to transform Wurster's blue, which is historically the first example of a stable radical ion in organic chemistry, into an exceptionally durable redoxmer molecule that persists over thousands of electrochemical cycles.**

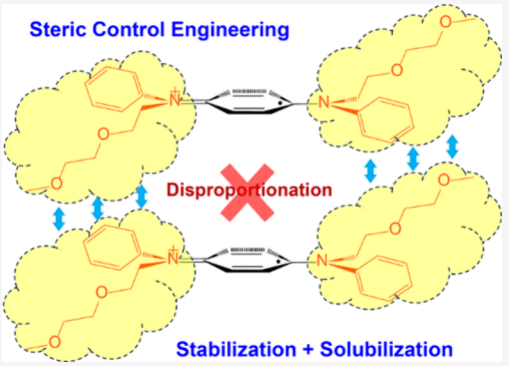

Using intermittent sources of power, such as solar and wind, requires large-scale energy storage to solve the challenge in balancing supply and demand. Redox flow batteries (RFBs) provide a promising approach to grid energy storage in which charge carriers (or redoxmer molecules) are dissolved in liquid electrolytes that are stored in external reservoirs and are pumped through electrodes during electrochemical cycling. This design leads to independent control over energy and power, with a potential for flexible scale-up. Over the past decade, there was rapid progress in the development and commercialization of aqueous RFBs.[1,2] Among them, vanadium RFBs are the most advanced systems, but the market penetration is hindered by high materials cost and limited energy density (25−30 Wh L^{-1}). Nonaqueous RFBs (NRFBs) present an attractive alternative by offering wider electrochemical stability windows (up to 5 V, compared to <1.5 V for aqueous systems) and more materials choices, potentially leading to energy-dense, cost-effective storage systems.[3,4] Organic redoxmers have gained momentum for NRFBs due to their structural diversity, molecular tailorability, and lower cost.[5−7] However, significant gaps still exist, as the current organic redoxmers are unable to satisfy the strict requirements for commercially competitive NRFBs.

Among these requirements, extremely high (by the standards of organic chemistry) chemical and electrochemical stabilities of their charged states remain the greatest concern, as it determines the cycle and calendar lives of the flow cell. Charging of organic molecules yields chemically reactive states whose compatibility with electrolyte needs to be carefully assessed.[8] Furthermore, these species may undergo cross reactions with each other and/or progenitor molecules, causing irreversible loss of capacity during electrochemical cycling and charge storage.[9−11] A particularly vexing parasitic reaction limiting redoxmer stability, especially at high concentrations, occurs when a redoxmer has more than one charged states involved in charge transfer equilibria. Due to such reactions, the unstable multiply charged states can be accessed even when the electrode potential is adjusted so that only singly charged molecules are generated at the electrode. The disproportionation of two singly charged molecules to a neutral progenitor and a doubly charged molecule is the common occurrence of such equilibria.

While thermodynamically the charge transfer equilibrium favors the singly charged states, irreversible decomposition of the less stable multiply charged states shifts this equilibrium toward the decomposition products, resulting in the overall

Received: September 4, 2024
Revised: October 12, 2024
Accepted: November 1, 2024
Published: November 5, 2024

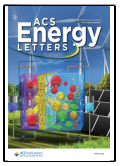

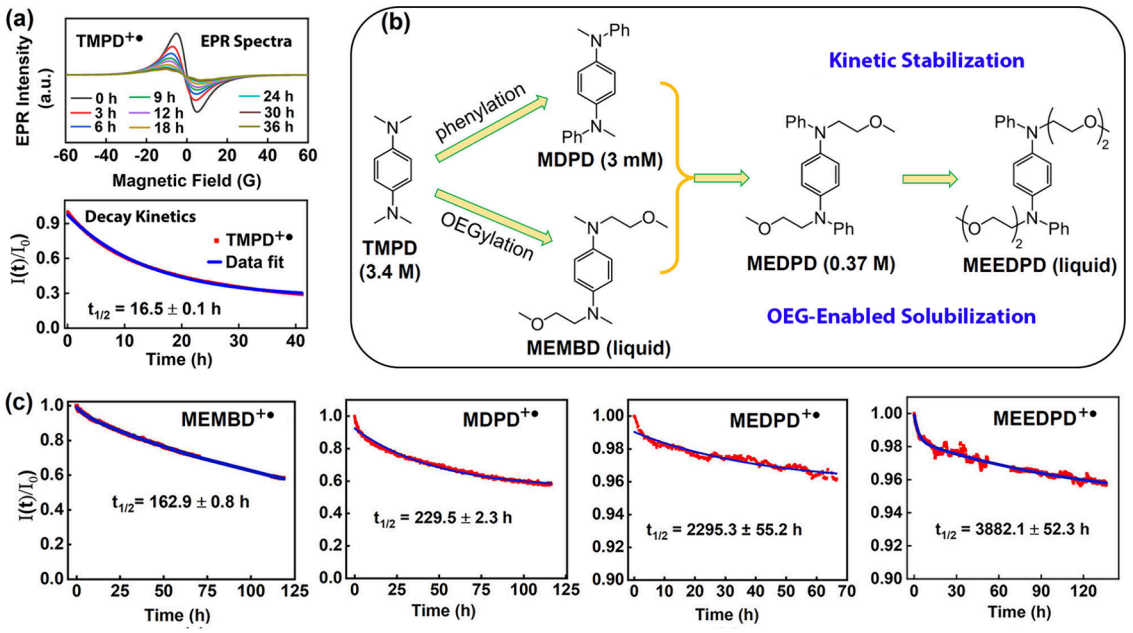

Figure 1. (a) Time-dependent EPR spectra (top) and fitted decay kinetics (bottom) of 50 mM TMPD$^{•+}$; (b) illustration of the progressive molecular design approach; (c) The decay kinetics of 50 mM MEMBD$^{•+}$, 2 mM MDPD$^{•+}$, 50 mM MEDPD$^{•+}$, and 50 mM MEEDPD$^{•+}$. In these panels, the red circles are the experimental $I(t)/I_0$, and the blue lines are the least-squares exponential fits. The low concentration of MDPD$^{•+}$ was used due to its low solubility in the electrolyte. The supporting electrolyte was 0.5 M LiTFSI in MeCN.

decay of charge carriers in solution. This reaction accelerates when the concentration of the redoxmer is increased or the redoxmers are clustered together as pendant groups in macromolecular scaffolds that are used to block membrane crossover.[12] A general strategy for suppressing these unwanted reactions is needed to achieve higher energy densities and longer cycle lives. Since the energetics of the charge transfer equilibria is "fixed" by the redox potentials that cannot be widely tuned, thermodynamics alone cannot suppress these parasitic reactions; thus, kinetic controls need to be engineered to slow them down.

Here we report a molecular design strategy to improve the stability of organic catholyte molecules (positive charge carriers) through suppression of the disproportionation of their radical cations (singly charged states). Historically, Wurster's blue, which is the trivial name for the oxidized *N*,*N*,*N*′,*N*′-tetramethyl-*p*-phenylenediamine (TMPD), was the first example of a radical ion identified by the great Leonor Michaelis.[13] TMPD derivatives have been evaluated in energy storage, e.g., as redox mediators in flow batteries and lithium−air batteries.[14,15] While TMPD can be useful in these applications, its use as a redoxmer in RFB electrolytes is limited by the tendency of TMPD$^{•+}$ to undergo disproportionation that yields the unstable dication (TMPD^{2+}, see below). This reaction occurs both in solution[16,17] and in solid TMPD$^{•+}$,[18,19] where it is facilitated by overlapping π-orbitals in the planar radical cations.[20−23] Aiming to suppress these unwanted reactions, we reasoned that the crowding of radical cations with bulky groups can prevent their close face-to-face approach, reducing the rate of the forward charge transfer. Synthetically, this steric protection was achieved by introducing phenyl and oligo(ethylene glycol) ether (OEG) substituents into the diamino groups. In symmetric flow cells, some of these sterically protected TMPD derivatives exhibit exceptional performance, resulting in 7,300 cycles with an overall capacity fade of 6% over 90 days.

Attracted by the high solubility of TMPD in polar organic solvents (3.2 M in acetonitrile and MeCN), we first studied this progenitor molecule but discovered that it was unsuitable for NRFBs. To demonstrate that, electron paramagnetic resonance (EPR) was used to characterize the decay kinetics of 50 mM TMPD$^{•+}$ in an electrolyte consisting of 0.5 M lithium bis(trifluoromethanesulfonyl)imide (LiTFSI) in MeCN. The first-derivative EPR spectra (Figure 1a) were doubly integrated to obtain the EPR signal $I(t)$ as a function of time. This quantity is proportional to the number of unpaired electrons in solution, and its decrease over time reflects the delayed decomposition of TMPD$^{•+}$ to the diamagnetic products. The obtained half-life ($t_{1/2}$) of 16.5 h is too short for practical use. Replacing Li^+ ion with organic cation *N*-methyl-*N*-butylpyrrolidinium ($PYR14^+$, to make possible significant increases of the redoxmer and salt concentrations, e.g., to 25 mol %) resulted in even shorter lifetime of 12 h (Figure S1a). This time was further reduced to <1 h when the concentration of TMPD$^{•+}$ increased to 25 mol % (Figure S1b) as can be expected for a disproportionation reaction. A series of liquid chromatography−mass spectrometry (LC-MS) and nuclear magnetic resonance (NMR) studies were carried out on the chemically prepared TMPD$^{•+}PF_6^-$ to elucidate its decomposition mechanisms (Sections S2). LC-MS detected the existence of proton (H^+) and *N*-methyl (Me^+) loss products in aged TMPD$^{•+}$ PF_6^- solutions (Figures S2−S3). A beige precipitate was collected from a concentrated TMPD$^{•+}$ PF_6^- electrolyte that was aged for 10 days. Combined NMR and LCMS studies suggest a polymeric product with a cationic backbone and PF_6^- anions as well as methylene ($-CH_2-$) groups bridging adjacent phenylenediamine rings (Figure S4). These analyses demonstrate the presence of side products formed from the dicationic form of TMPD (i.e., TMPD^{2+}), supporting a disproportionation-based decomposition pathway shown in Scheme S1. The unstable TMPD^{2+} undergoes facile deprotonation and *N*-demethylation reactions that shift the

https://doi.org/10.1021/acsenergylett.4c02449
ACS Energy Lett. 2024, 9, 5737−5743

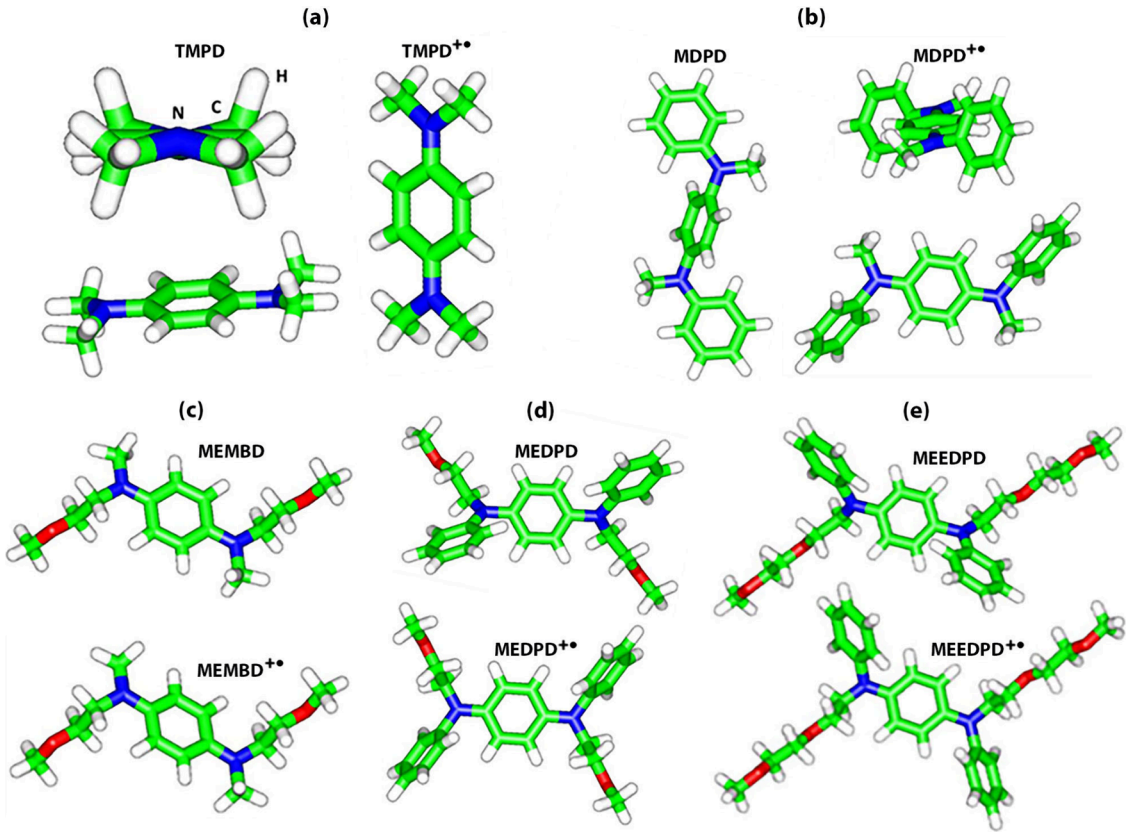

Figure 2. DFT calculations of gas-phase-optimized structures for (a) TMPD, (b) MDPD, (c) MEMBD, (d) MEDPD, and (e) MEEDPD in the neutral and singly charged states.

charge transfer equilibrium, indirectly causing rapid decay of the radical cation. From these observations, we hypothesized that substitution of TMPD at the nitrogen with bulky groups, including the *N*-phenyl groups that could not be easily eliminated from the dication, can both inhibit the disproportionation and improve the stability of dication, so that the overall reaction becomes shifted toward the radical cation. Since substitution of such bulky groups can decrease solubility of the redoxmer, ether chains were introduced into the amino groups as a second strategy to restore it.[24] Each modification was followed by a lifetime measurement using EPR spectroscopy to guide the design toward the most stable and soluble molecules.

Figure 1b illustrates the molecular design trajectory. First, TMPD was modified, separately, with the phenyl and 2′-methoxyethyl groups to afford *N*,*N*′-dimethyl-*N*,*N*′-diphenylbenzene-1,4-diamine (MDPD) and *N*,*N*′-bis(2′-methoxyethyl)-*N*,*N*′-dimethylbenzene-1,4-diamine (MEMBD), respectively. Based on both our calculations (see below) and EPR measurements (Figure S5), the *N*-phenyl ring protons have small hyperfine coupling constants (hfcc's) indicative of minimal π-conjugation over the radical cation, so these groups primarily serve as steric protection groups. As indicated by the EPR kinetics (Figures 1c and S6), $MDPD^{\bullet+}$ shows >10X improved chemical stability vs $TMPD^{\bullet+}$ with a $t_{1/2}$ of 230 h, suggesting that, even with the *N*-methyl groups retained, the introduction of *N*-phenyl groups considerably improves the stability of radical cation. However, as these are bulky and solvent-phobic groups, MDPD exhibits a low solubility of just 3.2 mM in MeCN. In contrast, the ether-derivatized MEMBD is a liquid at 25 °C and fully miscible with the solvent. Interestingly, $MEMBD^{\bullet+}$ also exhibits improved chemical stability ($t_{1/2}$ = 162 h) compared to $TMPD^{\bullet+}$, suggesting that crowding of the amino group in general improves the stability. In the next iteration, we combined the ether chains and *N*-phenyl groups in MEDPD, obtaining yet another 10-fold increase in the lifetime $t_{1/2}$ of 2,295 h (95 d). While such persistence would make MEDPD a good candidate for use in NRFBs, the solubility of this molecule was only 0.37 M in MeCN. In the final iteration, a longer ether chain was introduced to obtain *N*,*N*′-bis(2′-(2″-methoxyethoxy)ethyl)-*N*,*N*′-diphenylbenzene-1,4-diamine (MEEDPD). Like MEMBD, it is also liquid and readily miscible with MeCN, but unlike $MEMBD^{\bullet+}$, $MEEDPD^{\bullet+}$ was extremely stable, with $t_{1/2}$ of 3,882 h (162 d). This is one of the longest lifetimes recorded for a radical cation in solution, proving the viability of our approach. Equally importantly, all four TMPD derivatives were prepared using a one-step synthesis from inexpensive chemicals, suggesting an advantage of cost-effectiveness.

To better elucidate the mechanism for the observed stability, density functional theory (DFT) calculations were performed to determine the optimized molecular geometries and energetics of these redoxmers in different states of charge. These geometries are shown in Figure 2. In neutral TMPD, the two amino groups are puckered while the charged molecule becomes planar and highly symmetric (D_{2h}). Linus Pauling was the first to connect this symmetry and the exceptional stability of $TMPD^{\bullet+}$, reasoning that side reactions would break this symmetry, leading to higher reaction barriers.[13] With the *N*-substitution in the amino groups, both the neutral molecules and their charged states are no longer planar due to the steric strain introduced by these bulky groups. The strain causes

https://doi.org/10.1021/acsenergylett.4c02449
ACS Energy Lett. 2024, 9, 5737−5743

these groups to rotate out of the plane of phenylenediamine ring. The dihedral angles between the latter and the *N*-phenyl ring in neutral MDPD, MEDPD, and MEEDPD are 70−82° changing to 70−72° in their charged states (Table S1 in Section S4). Likewise, for the *N*-ether groups, the corresponding dihedral angles are 45−56° in the neutral states and 25−40° in the charged states. These propeller-like conformations make such groups efficient steric protectors, explaining their ability to suppress disproportionation.

There is another interesting structural property of these molecules that is less obvious: as the two amines are identically substituted, the molecule can be either mirror- or centrosymmetric (the C_2 and C_i states, respectively). In the neutral and singly charged MEMBD and MDPD, these two conformers are almost degenerate in energy, so the molecules can flex between the two conformations. In contrast, MEDPD and MEEDPD are conformationally locked in the mirror symmetry in all states of charge. While there is the usual chain dynamics in the ether groups, the *bis*-*N*-phenyl−phenylenediamine core of these molecules is "frozen." This property makes the charged states more rigid and less prone to the symmetry-preserving reactions like the loss of *N*-alkyl groups, recapitulating Pauling's rationale for the exceptional stability of $TMPD^{\bullet+}$. A good correspondence of magnetic parameters computed for symmetric $MEDPD^{\bullet+}$ and $MEEDPD^{\bullet+}$ with the ones obtained for EPR spectroscopy (Figure S5) strongly supports the high symmetry of these radical cations, validating our structural insights.

While the exceptional stability of electrochemically generated charged species is obviously necessary for long-term charge storage in extant reservoirs, it is equally important for cycling stability. These two metrics do not always correlate as there are parasitic reactions that occur only near the electrodes.[25] The electrochemical behaviors of the TMPD derivatives were first investigated by using cyclic voltammetry (CV). Both $1e^-$ and $2e^-$ oxidation waves are observed (Figure S7 and Table S2), corresponding to the formation of a radical cation and a dication, respectively. On the time scale of the CV scans, these electrochemical reactions are reversible, with the exception of $2e^-$ oxidation of MDPD. The large energy gap between the $1e^-$ and $2e^-$ redox reactions (>0.5 V for all molecules) explains why the charge transfer equilibrium in the solvent bulk is strongly shifted toward the radical cation. Figure 3 compares cyclic voltammograms for one-electron oxidation

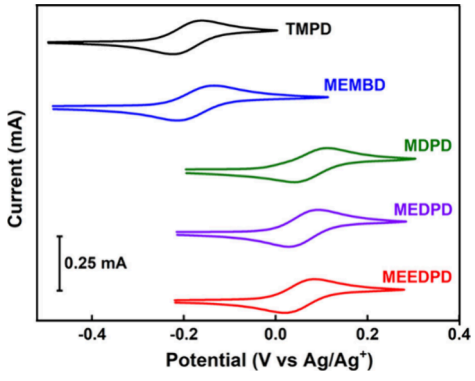

Figure 3. Cyclic voltammograms for $1e^-$ oxidation of TMPD, MEMBD, MEDPD, and MEEDPD at 5 mM and MDPD at 2 mM obtained with a sweep rate of 100 mV s^{-1}. The supporting electrolyte was 0.5 M LiTFSI in MeCN.

of a 5 mM redoxmer in 0.5 M LiTFSI/MeCN at a sweep rate of 100 mV s^{-1}. TMPD has a redox potential of −0.206 V vs Ag/Ag^+. Substituting the *N*-methyl with ether chains in MEMBD does not change the redox potential appreciably, but incorporating the *N*-phenyl groups increases it by over 0.25 V. As shown in Figure S8, the experimental $1e^-$ and $2e^-$ redox potentials linearly correlate with the number of heteroatoms in the substituent groups and the presence of the *N*-phenyl groups. For the $2e^-$ oxidation, this trend is reproduced in our DFT calculations, but for $1e^-$ oxidation the correspondence is less exact, although the more positive potential for *N*-phenyl derivatives is reproduced in these calculations, too.

The CVs at different scan rates were obtained to estimate the diffusion coefficients by the Randles−Sevick analysis (Figures S9−S13).[26] TMPD shows the highest diffusivity of 12.7×10^{-6} cm^2 s^{-1}, while the bulkier derivatives are slower, as can be expected from their relative size. The electron transfer rate constants for the redoxmers were calculated using the Nicholson's method[27] and found to be $\approx 10^{-2}$ cm s^{-1} for all molecules.

As the charged MEEDPD has the longest lifetime, it was selected for further electrochemical experiments. Due to the lack of selective membranes for NRFBs, assessing the cycling stability of molecular redoxmers has been a challenge, as it is always compromised by migration of the small molecules across the membrane. In this regard, symmetric flow cells, where the same molecule in different states of charge is present in both cell compartments, have been used to minimize such interference.[28,29] In our test, a symmetric cell with a Daramic porous separator (Figure 4a) was used. MEEPD was electrochemically charged to 50% theoretical capacity using bulk electrolysis (Figure S14) and then introduced to both compartments of a symmetric flow cell. Figure 4b,c shows the time profiles for voltage and capacity for a symmetric flow cell galvanostatically cycled at different current densities, with the cycles interrupted at attainment of set voltages. An area-specific resistance of 9.4 Ω cm^2 was measured for this cell by using electrochemical impedance spectroscopy (EIS, Figure S15). As the current density increases from 20 to 50 mA cm^{-2}, the cell polarization increases and the material utilization decreases from 85% to 69%. The long-term cycling is illustrated in Figure 4d. At a current density of 50 mA cm^{-2}, each cycle took ≈18 min. High Coulombic efficiency (CE) was maintained over 7,300 cycles with the mean value of 99.7%. During the cycling, volume losses were observed due to the slow evaporation of MeCN through the seals around the membrane. This loss causes increased resistance through greater association of electrolyte ions, so periodically a fixed volume of the solvent was added to each cell compartment, which is denoted as event "A" in Figure 4d. In addition, we periodically rebalanced the electrolyte by mixing the solutions from the two compartments and then dividing them equally between them (denoted as event "R").[30] The nearly identical voltage profile after each such step (Figure S16) suggests the effectiveness of this procedure (which is also practiced for aqueous vanadium flow cells).[30] With this periodic maintenance, a capacity retention of 94% was obtained after 90 days, corresponding to an average rate for capacity fade of 0.067% per day of cycling.

The symmetric flow cell was then evaluated at a higher redoxmer concentration (Figure S17) that is more typical of practical applications. We remind ourselves that the rate of disproportionation increases with the concentration of radical

https://doi.org/10.1021/acsenergylett.4c02449
ACS Energy Lett. 2024, 9, 5737−5743

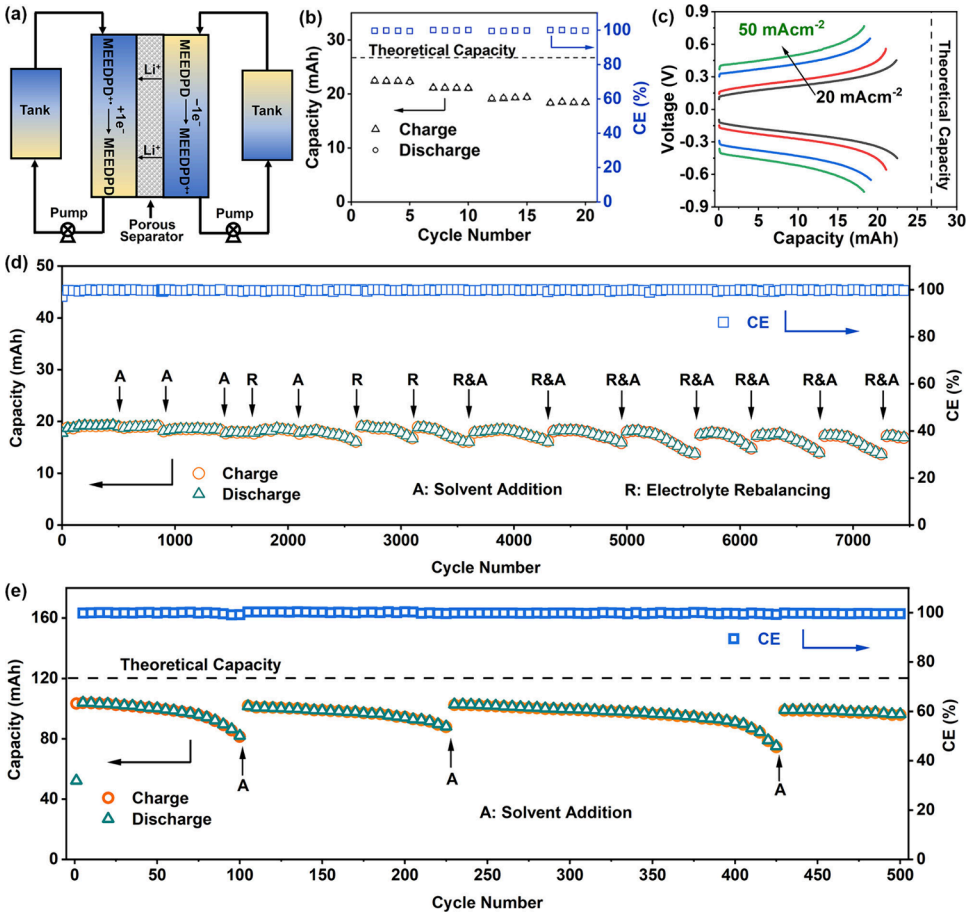

Figure 4. Symmetric MEEDPD flow cells: (a) Schematic illustration of a symmetric flow cell; (b) Charge and discharge capacities and (c) voltage curves of the 0.1 M symmetric flow cell at different current densities; (d) Long cycling of the 0.1 M symmetric flow cell at 50 mA cm^{-2}; (e) Long cycling of the 0.5 M symmetric flow cell at 50 mA cm^{-2}.

cations in electrolyte, so this test is essential in demonstration that our design strategy has addressed the problem. Figure 4e shows capacity fade and CE profiles for a 0.5 M MEEDPD symmetric flow cell operated at a current density of 50 mA cm^{-2}. Due to a higher concentration of electrolyte, solvent evaporation caused still more capacity loss due to a steeper decrease in ionic conductivity caused by the solvent removal from the electrolyte. To compensate, a fixed volume of solvent (12 mL) was added to each cell compartment every 8 days. Each such solvent addition restored the lost capacity almost to the initial level (Figure S18). The 0.5 M symmetric flow cell showed stable cycling over 500 cycles, with an overall capacity retention of 92.5% over 32.5 days. With the periodic solvent replacements, the cell resistance slowly increased by 30% over this period of time (Figure S19).

Such stable cycling at a high concentration implies that the disproportionation reactions have been largely suppressed in this redox system, and the cycling lifetime is limited by the imperfect cell design. Also worth mentioning is that the cycling of MEEDPD is impervious to air leaks that are difficult to avoid in a commercial setting. To show that, a symmetric H-cell containing 2 mM MEEDPD was operated *in air*, yielding the average CE of 99.1% over 200 cycles (Figure S20). Such oxygen resistance is rarely seen for radical ions.

In full cells, the cycling of redoxmers is affected by crossover between the cell compartments: the redox-active molecules and products of their decomposition eventually migrate across the membrane, causing parasitic reactions. Given the mild redox potential of TMPD derivatives, to obtain cell voltage >1 V, low-potential anolytes such as 2,1,3-benzothiadiazole (BzNSN) are required, whose charged states are highly reactive organic bases.[10,31] As shown in Figure S21, a MEEDPD/BzNSN flow cell using mixed electrolytes in both cell compartments exhibits a continuous capacity loss over 160 cycles, which is a small fraction of the cycling lifetime observed for MEEDPD in symmetric cells. Based on our prior study,[10] we believe decomposition of BzNSN$^{\bullet-}$ was the major factor that caused capacity degradation in the full cell test. Given the dearth of suitable low potential, yet stable anolytes, we were unable to pair MEEDPD with an anolyte that would showcase its exceptional stability while yielding voltages >1 V.

To conclude, we have demonstrated how an organic catholyte can be stabilized through the suppression of charge transfer equilibria shifted toward the byproducts due to involvement of unstable multiply charged states. These reactions are a hurdle to achieving high energy densities in all redoxmer systems. Since the free energy of charge equilibria cannot be widely tuned, only kinetic control was possible. We demonstrate how to achieve this control by (i) engineering steric hindrance preventing close approach between the charged molecules, (ii) slowing down the decomposition of a multiply charged state by strengthening bonds between the redox core and the bulky groups, and (iii) using molecules that are conformationally locked in their symmetric states in all

https://doi.org/10.1021/acsenergylett.4c02449
ACS Energy Lett. 2024, 9, 5737−5743

states of charge. A combination of these three approaches allowed us to transform a relatively unstable radical cation (Wurster's blue) to one of the most stable organic catholytes identified so far, to the extent that we cannot find a stable low-potential anolyte to pair it with in full cells. Two more properties were engineered into this molecule, one intentionally (solubility) and another indvertantly (oxygen resistance). To obtain higher solubility, ether chains were used to obtain a liquid catholyte that is miscible with the electrolyte. Our molecular design shows how beneficial traits can be combined in a small redox active molecule to obtain exceptional performance. It also suggests that unexpected and practically interesting properties can occur in such molecules that are not part of the planning.

Finally, we note that charge equilibria often prevent the use of redox-active molecules as pendant groups in oligomer and polymer scaffolds, where these charged groups can be close to each other, accelerating their decay. While this tendency can be addressed by making rigid scaffolds, preventing the encounters, such scaffolds often suffer from low solubility and synthetic complexity. As these macromolecular scaffolds can be used with size-selective nanoporous membranes to block the crossover, overcoming this common hurdle is pivotal for further evolution of the "redoxmer" concept that presently offers the only viable solution to the crossover in the NRFBs.

■ ASSOCIATED CONTENT

Supporting Information

The Supporting Information is available free of charge at https://pubs.acs.org/doi/10.1021/acsenergylett.4c02449.

Detailed decomposition analysis of $TMPD^{\bullet+}$, experimental procedures, materials synthesis, and additional figures and tables, including EPR spectra and kinetics, UV−vis spectra, LC-MS, NMR spectra, CV curves, DFT calculations, EIS plots, voltage curves, and flow cell performance (PDF)

■ AUTHOR INFORMATION

Corresponding Authors

Ilya A. Shkrob − *Joint Center for Energy Storage Research, Argonne National Laboratory, Lemont, Illinois 60439, United States; Chemical Sciences and Engineering Division, Argonne National Laboratory, Lemont, Illinois 60439, United States;* orcid.org/0000-0002-8851-8220; Email: shkrob@anl.gov

Xiaoliang Wei − *School of Mechanical Engineering, Purdue University, Indianapolis, Indiana 46202, United States;* orcid.org/0000-0002-7692-2357; Email: wei304@purdue.edu

Lu Zhang − *Joint Center for Energy Storage Research, Argonne National Laboratory, Lemont, Illinois 60439, United States; Chemical Sciences and Engineering Division, Argonne National Laboratory, Lemont, Illinois 60439, United States;* Email: zhanglu77@gmail.com

Authors

Xiaoting Fang − *Joint Center for Energy Storage Research, Argonne National Laboratory, Lemont, Illinois 60439, United States; Chemical Sciences and Engineering Division, Argonne National Laboratory, Lemont, Illinois 60439, United States; School of Mechanical Engineering, Purdue University, Indianapolis, Indiana 46202, United States*

Zhiguang Li − *Joint Center for Energy Storage Research, Argonne National Laboratory, Lemont, Illinois 60439, United States; Chemical Sciences and Engineering Division, Argonne National Laboratory, Lemont, Illinois 60439, United States; School of Mechanical Engineering, Purdue University, Indianapolis, Indiana 46202, United States*

Lifan Zeng − *Chemical Genomics Core, School of Medicine, Indiana University, Indianapolis, Indiana 46202, United States*

Heonjae Jeong − *Joint Center for Energy Storage Research, Argonne National Laboratory, Lemont, Illinois 60439, United States; Materials Science Division, Argonne National Laboratory, Lemont, Illinois 60439, United States;* Present Address: Department of Electronic Engineering, Gachon University, 1342 Seongnam-daero, Seongnam, Gyeonggi 13120, South Korea; orcid.org/0000-0003-4452-049X

Diqing Yue − *School of Mechanical Engineering, Purdue University, Indianapolis, Indiana 46202, United States;* orcid.org/0000-0002-9162-9810

Lily A. Robertson − *Joint Center for Energy Storage Research, Argonne National Laboratory, Lemont, Illinois 60439, United States; Chemical Sciences and Engineering Division, Argonne National Laboratory, Lemont, Illinois 60439, United States;* orcid.org/0000-0002-8784-0568

Yuyue Zhao − *Chemical Sciences and Engineering Division, Argonne National Laboratory, Lemont, Illinois 60439, United States; School of Mechanical Engineering, Purdue University, Indianapolis, Indiana 46202, United States*

Lei Cheng − *Joint Center for Energy Storage Research, Argonne National Laboratory, Lemont, Illinois 60439, United States; Materials Science Division, Argonne National Laboratory, Lemont, Illinois 60439, United States;* orcid.org/0000-0002-3902-1680

Complete contact information is available at: https://pubs.acs.org/10.1021/acsenergylett.4c02449

Author Contributions

$^{\nabla}$(X.F. and Z.L.) These authors contributed equally.

Notes

The authors declare no competing financial interest.

■ ACKNOWLEDGMENTS

This work was partially supported by the Joint Center for Energy Storage Research (JCESR), an Energy Innovation Hub funded by the U.S. Department of Energy, Office of Science, Basic Energy Sciences. The authors also thank financial support from the U.S. National Science Foundation (Award No. CHE-2055222). The submitted manuscript has been created by UChicago Argonne, LLC, Operator of Argonne National Laboratory ("Argonne"). Argonne, a U.S. Department of Energy Office of Science laboratory, is operated under Contract No. DE-AC02-06CH11357. The U.S. Government retains for itself, and others acting on its behalf, a paid-up nonexclusive, irrevocable worldwide license in said article to reproduce, prepare derivative works, distribute copies to the public, and perform publicly and display publicly, by or on behalf of the Government.

■ REFERENCES

(1) Soloveichik, G. L. Flow batteries: current status and trends. *Chem. Rev.* **2015**, *115*, 11533−11558.

(2) Winsberg, J.; Hagemann, T.; Janoschka, T.; Hager, M. D.; Schubert, U. S. Redox-flow batteries: from metals to organic redox-active materials. *Angew. Chem., Int. Ed.* **2017**, *56*, 686−711.
(3) Li, M.; Rhodes, Z.; Cabrera-Pardo, J. R.; Minteer, S. D. Recent advancements in rational design of non-aqueous organic redox flow batteries. *Sustain. Energy Fuels* **2020**, *4*, 4370−4389.
(4) Gong, K.; Fang, Q. R.; Gu, S.; Li, S. F. Y.; Yan, Y. S. Nonaqueous redox-flow batteries: organic solvents, supporting electrolytes, and redox pairs. *Energy Environ. Sci.* **2015**, *8*, 3515−3530.
(5) Wei, X. L.; Pan, W. X.; Duan, W. T.; Hollas, A.; Yang, Z.; Li, B.; Nie, Z. M.; Liu, J.; Reed, D.; Wang, W.; Sprenkle, V. Materials and Systems for Organic Redox Flow Batteries: Status and Challenges. *ACS Energy Lett.* **2017**, *2*, 2187−2204.
(6) Ding, Y.; Zhang, C. K.; Zhang, L. Y.; Zhou, Y. E.; Yu, G. H. Molecular engineering of organic electroactive materials for redox flow batteries. *Chem. Soc. Rev.* **2018**, *47*, 69−103.
(7) Luo, J. A.; Hu, B.; Hu, M. W.; Zhao, Y.; Liu, T. L. Status and Prospects of Organic Redox Flow Batteries toward Sustainable Energy Storage. *ACS Energy Lett.* **2019**, *4*, 2220−2240.
(8) Wei, X. L.; Xu, W.; Huang, J. H.; Zhang, L.; Walter, E.; Lawrence, C.; Vijayakumar, M.; Henderson, W. A.; Liu, T. B.; Cosimbescu, L.; Li, B.; Sprenkle, V.; Wang, W. Radical Compatibility with Nonaqueous Electrolytes and Its Impact on an All-Organic Redox Flow Battery. *Angew. Chem., Int. Ed.* **2015**, *54*, 8684−8687.
(9) Zhang, J.; Shkrob, I. A.; Assary, R. S.; Tung, S. o.; Silcox, B.; Curtiss, L. A.; Thompson, L.; Zhang, L. Toward Improved Catholyte Materials for Redox Flow Batteries: What Controls Chemical Stability of Persistent Radical Cations? *J. Phys. Chem. C* **2017**, *121*, 23347−23358.
(10) Zhang, J. J.; Huang, J. H.; Robertson, L. A.; Assary, R. S.; Shkrob, I. A.; Zhang, L. Elucidating Factors Controlling Long-Term Stability of Radical Anions for Negative Charge Storage in Nonaqueous Redox Flow Batteries. *J. Phys. Chem. C* **2018**, *122*, 8116−8127.
(11) Armstrong, C. G.; Toghill, K. E. Stability of molecular radicals in organic non-aqueous redox flow batteries: A mini review. *Electrochem. Commun.* **2018**, *91*, 19−24.
(12) Lai, Y. Y.; Li, X.; Zhu, Y. Polymeric Active Materials for Redox Flow Battery Application. *ACS Appl. Polym. Mater.* **2020**, *2*, 113−128.
(13) Michaelis, L.; Schubert, M. P.; Granick, S. The Free Radicals of the Type of Wurster's Salts. *J. Am. Chem. Soc.* **1939**, *61*, 1981−1992.
(14) Zhu, Y. G.; Du, Y.; Jia, C.; Zhou, M.; Fan, L.; Wang, X.; Wang, Q. Unleashing the power and energy of LiFePO4-based redox flow lithium battery with a bifunctional redox mediator. *J. Am. Chem. Soc.* **2017**, *139*, 6286−6289.
(15) Chen, Y.; Gao, X.; Johnson, L. R.; Bruce, P. G. Kinetics of lithium peroxide oxidation by redox mediators and consequences for the lithium-oxygen cell. *Nat. Commun.* **2018**, *9*, 1−6.
(16) Störle, C.; Eyer, P. Reactions of the Wurster's blue radical cation with thiols, and some properties of the reaction products. *Chem.-Biol. Interact.* **1991**, *78*, 333−346.
(17) Chaka, G.; Bakac, A. Two-electron oxidation of *N*, *N*, *N*′,*N*′-tetramethylphenylenediamine with a chromium(V) salen complex. *Dalton Trans.* **2009**, *2009*, 318−321.
(18) Pott, G. T.; Kommandeur, J. Magnetic Transition of Wurster's Bluo Perchlorate. I. The Low-Temperature Phase. *J. Chem. Phys.* **1967**, *47*, 395−401.
(19) Stanic, P.; Niksic-Franjic, I.; Molcanov, K. Pancake-Bonded Dimers of Semiquinone Radical Cations of N,N,N′,N′-Tetramethyl-p-phenylenediamine (Wurster's Blue). *Cryst. Growth Des.* **2023**, *23*, 4571−4579.
(20) Grilj, J.; Laricheva, E. N.; Olivucci, M.; Vauthey, E. Fluorescence of Radical Ions in Liquid Solution: Wurster's Blue as a Case Study. *Angew. Chem., Int. Ed.* **2011**, *50*, 4496−4498.
(21) Hausser, K. H.; Murrell, J. N. Pi Complexes between Organic Free Radicals. *J. Chem. Phys.* **1957**, *27*, 500−504.
(22) Uemura, K.; Nakayama, S.; Seo, Y.; Suzuki, K.; Ooshika, Y. The Temperature Dependence of the Absorption Spectra of Wurster's Blue-type Ion Radicals. *Bull. Chem. Soc. Jpn.* **1966**, *39*, 1348.
(23) Kimura, K.; Yamada, H.; Tsubomura, H. Electronic Absorption Spectra of Dimers of *p*-Benzosemiquinone Anion and Wurster's Cations in Solution. *J. Chem. Phys.* **1968**, *48*, 440−444.
(24) Huang, J. H.; Cheng, L.; Assary, R. S.; Wang, P. Q.; Xue, Z.; Burrell, A. K.; Curtiss, L. A.; Zhang, L. Liquid Catholyte Molecules for Nonaqueous Redox Flow Batteries. *Adv. Energy Mater.* **2015**, *5*, 1401782.
(25) Silcox, B.; Zhang, J.; Shkrob, I. A.; Thompson, L.; Zhang, L. On Transferability of Performance Metrics for Redox-Active Molecules. *J. Phys. Chem. C* **2019**, *123*, 16516−16524.
(26) Compton, R. G.; Banks, C. E. *Understanding voltammetry*; World Scientific, 2018.
(27) Luo, J.; Sam, A.; Hu, B.; DeBruler, C.; Wei, X. L.; Wang, W.; Liu, T. L. Unraveling pH dependent cycling stability of ferricyanide/ferrocyanide in redox flow batteries. *Nano Energy* **2017**, *42*, 215−221.
(28) Goulet, M. A.; Aziz, M. J. Flow Battery Molecular Reactant Stability Determined by Symmetric Cell Cycling Methods. *J. Electrochem. Soc.* **2018**, *165*, A1466−A1477.
(29) Milshtein, J. D.; Kaur, A. P.; Casselman, M. D.; Kowalski, J. A.; Modekrutti, S.; Zhang, P. L.; Harsha Attanayake, N.; Elliott, C. F.; Parkin, S. R.; Risko, C.; Brushett, F. R.; Odom, S. A. High current density, long duration cycling of soluble organic active species for non-aqueous redox flow batteries. *Energy Environ. Sci.* **2016**, *9*, 3531−3543.
(30) Luo, Q. T.; Li, L. Y.; Wang, W.; Nie, Z. M.; Wei, X. L.; Li, B.; Chen, B. W.; Yang, Z. G.; Sprenkle, V. Capacity Decay and Remediation of Nafion-based All-Vanadium Redox Flow Batteries. *ChemSusChem* **2013**, *6*, 268−274.
(31) Duan, W. T.; Huang, J. H.; Kowalski, J. A.; Shkrob, I. A.; Vijayakumar, M.; Walter, E.; Pan, B. F.; Yang, Z.; Milshtein, J. D.; Li, B.; Liao, C.; Zhang, Z. C.; Wang, W.; Liu, J.; Moore, J. S.; Brushett, F. R.; Zhang, L.; Wei, X. L. "Wine-Dark Sea" in an Organic Flow Battery: Storing Negative Charge in 2,1,3-Benzothiadiazole Radicals Leads to Improved Cyclability. *ACS Energy Lett.* **2017**, *2*, 1156−1161.

https://doi.org/10.1021/acsenergylett.4c02449
ACS Energy Lett. 2024, 9, 5737−5743